On the fabrication of all-glass optical fibers from crystals

J. Ballato,[1,a)] T. Hawkins,[1] P. Foy,[1] B. Kokuoz,[1] R. Stolen,[1] C. McMillen,[1,2]
M. Daw,[1,3] Z. Su,[1,3] T. M. Tritt,[1,3] M. Dubinskii,[4] J. Zhang,[4] T. Sanamyan,[4] and
M. J. Matthewson[5]

[1]*Center for Optical Materials Science and Engineering Technologies (COMSET), School of Materials Science and Engineering, Clemson University, Clemson, South Carolina 29634, USA*
[2]*Department of Chemistry, Clemson University, Clemson, South Carolina 29634, USA*
[3]*Department of Physics and Astronomy, Clemson University, Clemson, South Carolina 29634, USA*
[4]*US Army Research Laboratory, AMSRD-ARL-SE-EO 2800 Powder Mill Road, Adelphi, Maryland 20783, USA*
[5]*Department of Materials Science and Engineering, Rutgers, The State University of New Jersey, 607 Taylor Road, Piscataway, New Jersey 08854, USA*

The highly nonequilibrium conditions under which optical fibers conventionally are drawn afford considerable, yet underappreciated, opportunities to realize fibers comprised of novel materials or materials that themselves cannot be directly fabricated into fiber form using commercial scalable methods. Presented here is an in-depth analysis of the physical, compositional, and selected optical properties of silica-clad erbium-doped yttrium aluminosilicate glass optical fibers derived from undoped, 0.25, and 50 wt % Er^{3+}-doped yttrium aluminum garnet (YAG) crystals. The YAG-derived fibers were found to be noncrystalline as evidenced by x-ray diffraction and corroborated by spectroscopic measurements. Elemental analysis across the core/clad interface strongly suggests that diffusion plays a large role in this amorphization. Despite the noncrystalline nature of the fibers, they do exhibit acceptable low losses ($\sim$0.15–0.2 dB/m) for many applications, broad-band emissions in the near-infrared, and enhanced thermal conductivity along their length while maintaining equivalent mechanical strength with respect to conventional silica optical fibers. Further, considerably higher rare-earth doping levels are realized than can be achieved by conventional solution or vapor-phase doping schemes. A discussion of opportunities for such approaches to nontraditional fiber materials is presented. © *2009 American Institute of Physics.*
[DOI: 10.1063/1.3080135]

I. INTRODUCTION

The vast majority of optical fiber is made from combinations of core and clad compositions that are variations on the same theme. In other words, the cladding and core are essentially the same material but with a minor compositional perturbation to adjust the refractive indices to permit light confinement and guidance. Such similarities between core and clad materials yield additional benefits such as amenability to codrawing and well-matched thermal expansion coefficients. However, using the same family of core and clad materials severely restricts the choice of materials from which fibers can be made. Over the years, there have been occasional successes in fabricating optical fibers comprised of considerably dissimilar materials including all-glass fibers,[1–3] crystalline fibers,[4,5] and glass-clad crystal core fibers.[6,7] However, the trend within the optical fiber community has been more focused on developing fiber geometries of ever-greater complexity than on new combinations of materials that could enable additional and value-added optical and optoelectronic functions.

This paper provides a thorough material characterization of optical fibers prepared from a crystalline starting material for the core; specifically Er^{3+}-doped yttrium aluminum gar-

net (YAG). The choice of Er:YAG was due to recent work using conventional fiber draw techniques to make glass-clad fibers with cores purportedly containing (chromium doped) YAG.[8,9] In those reports, a single crystal of (Cr doped) YAG was sleeved inside a silica glass tube and drawn into fiber using a conventional fiber draw approach. The core material is molten at the temperature where the glass capillary tube (and optical cladding) softens.

In the present work, silica glass-clad fibers of varying diameters were drawn from preforms containing undoped and erbium-doped YAG single crystals in the core. These preforms were drawn into fiber at temperatures above the melting point of the YAG core crystal. X-ray diffraction was used as the primary tool to examine crystallinity in the resultant fiber core. Optical absorption and emission measurements of rare-earth-doped fiber samples were made to provide a secondary indication of crystallinity since spectral linewidths broaden in amorphous hosts. Diffusion from cladding to core, which is likely at the high draw temperatures, was investigated using energy dispersive x ray (EDX) for elemental analysis. Lastly, since the ultimate goal is the practical use of the fiber, both the strength and the thermal conductivity of the drawn fibers—properties important for high-power amplifier applications—were studied.

Although our initial hope was that the fibers would possess some degree of YAG crystallinity, the resultant cores

---

a)Electronic mai: jballat@clemson.edu.

105, 053110-1

were found to be a fully amorphous yttrium-aluminosilicate glass. However, the fibers did exhibit beneficial physical and optical properties that make them of potential interest as optical amplifiers and lasers. The results are insightful into how this molten core process can be a valuable processing approach to realizing optical fibers with cores comprising materials that are either highly dissimilar from the cladding or would not themselves be amendable to the direct fabrication into fiber form.

II. EXPERIMENTAL PROCEDURES

Commercial grade single crystals of YAG (undoped 0.25 wt % Er doped and 50 wt % Er doped) for use in the core of the preforms were provided by Northrop Grumman Synoptics (Charlotte, NC). The YAG boule was core-drilled (Ceramare, Piscataway, NJ) into rods measuring 3 mm in diameter and approximately 40 mm in length. Optical quality silica glass (F300) for use as the cladding was purchased from Heraeus Tenevo (Buford, GA).

A series of the silica glass capillary tubes was drawn to differing sizes and sleeved within one another to yield a preform having an outer diameter of 51 mm and an inner diameter of 3 mm. This preform was then fire polished using an internal procedure. The YAG core rod then was placed in the center of the capillary cladding glass preform.

For each of the YAG compositions (undoped, 0.25%, and 50% Er:YAG) from which the preform was prepared a series of large fibers (canes) was drawn to varying diameters in order to quantify diffusion effects on the core composition. Following the collection of these canes, each YAG-derived fiber was drawn down to 125 μm, coated with a single layer of UV curable polymer (DSM Desolite 3471–3-14), and about 1 km was collected on a spool for a variety of subsequent measurements. All fibers were drawn at approximately 2025 °C using the Heathway fiber draw tower at Clemson University.

A. X-ray diffraction

Powder x-ray diffraction patterns were collected using a Scintag XDS 2000-2 powder diffractometer with Cu $K\alpha$ radiation ($\lambda = 1.5418$ Å) and a solid-state Ge detector. Diffraction patterns were collected from 5° to 65° in 2-theta in 0.03° steps at rates of 2–10 s/step. Samples were analyzed both as intact fibers and as pulverized powders. Further, in some cases both the core and the silica cladding were analyzed and in selected cases, the silica cladding was partially removed by etching in dilute HF acid.

B. Microscopic and elemental analysis

Prior to examination the fiber ends were mechanically polished with 600 grit silicon carbide (SiC) bonded paper. Uncoated samples were investigated using a Hitachi 3400 N scanning electron microscope. EDX spectroscopy was performed to examine the distribution of major elements (Si, O, Al, Y, and Er). Elemental compositions were measured at several locations along a line traversing the core. The micro-scope was operated at 20 or 30 kV and 10 mm working distance under variable pressure. EDX typically has a spatial resolution of about 1 μm.

C. Fiber attenuation and spectroscopic measurements

Baseline fiber attenuation measurements were performed using a Photon Kinetic 2500 optical fiber analysis system. In this case the attenuation wavelength dependence was measured with 10 nm wavelength increments. The 5 and 10 m cutback lengths were used for the fiber drawn using the undoped YAG crystal and 0.25 wt % erbium-doped YAG crystal, respectively.

In order to characterize the fibers spectroscopically, with the purpose of determining whether they have crystalline or amorphous structure, significantly higher (than 10 nm) spectral resolution is required. For this purpose fiber absorption was measured by using the standard "cutback" technique, whereby the light from the fiber-coupled "white light" source (Yokogawa AQ4305 white light source) transmitted through the fiber under investigation was spectrally analyzed by the AQ6370 optical spectrum analyzer (OSA). Spectrally dispersed, with the 1 nm OSA resolution, light intensities (log scale) separately measured on the samples of 2.688 m and 0.653 m long were subtracted and then divided by the differential length (2.035 m cutback) in order to infer the true dB/m core absorption value.

The $^4I_{13/2} - {}^4I_{15/2}$ Er^{3+} fluorescence spectra were measured using an Acton 2500i monocromator, thermoelectrically cooled InGaAs detector, and lock-in amplifier. The monochromator slits were chosen to provide a resolution better than 0.35 nm. Fluorescence was always collected perpendicular to the fiber axis. This collection mode, even though it does not offer a higher signal-to-noise ratio, does avoid spectral distortions due to fluorescence emission reabsorption of waveguided light. It also helps us to avoid systematic errors in lifetime measurements associated with fluorescence radiation trapping. All obtained spectra were corrected for the spectral response of the entire system. For spectral scanning fluorescence was excited by electrically chopped 976 nm fiber-coupled GaAs diode laser. The same setup was utilized for fluorescence lifetime measurements, except a short-pulse (~10 ns) excitation source, frequency-doubled Nd:YAG laser at 532 nm, was used in this case. Time resolution for the lifetime measurements was 3 μs. The lifetime was measured by a Tektronix digital oscilloscope with the averaging used for signal-to-noise improvement.

D. Thermal conductivity measurements

The geometry and size of optical fibers is not conducive to conventional four-probe steady state thermal conductivity measurement methods. Therefore, the parallel thermal conductance system was used to measure the thermal conductance along the length of the samples at temperatures ranging from 10 K to room temperature.[10] Samples were cooled with a cryocooler to the desired temperature set by the user at an adjustable cooling rate then warmed up while the system begins to take the data with preset temperature intervals. For

(a)

Spectrum 1

200μm   (b)
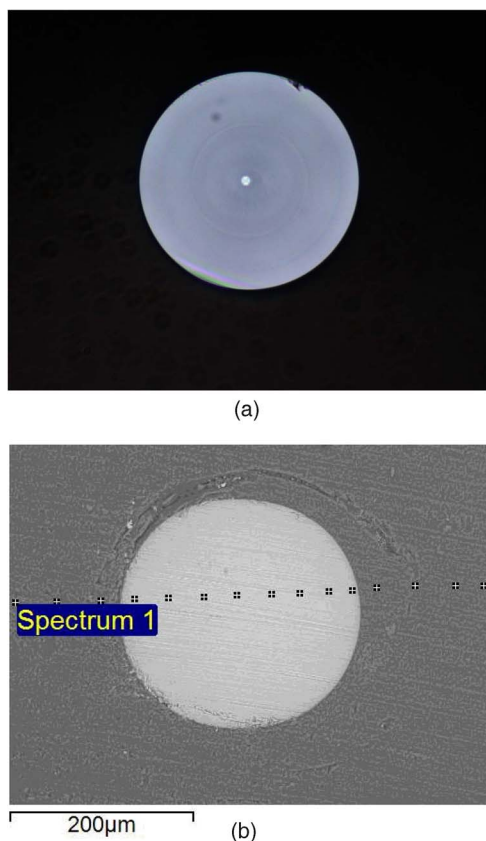
FIG. 1. (Color online) Optical (a) and electron microscopic (b) images of different representative fibers drawn from a YAG starting core crystal. The optical micrograph (a) is of a fiber with a 125 μm outer diameter. The electron micrograph (b) is of a fiber drawn to a diameter such that the core was about 250 μm. The points marked across the core region (b) indicate where elemental analysis was performed (see Figs. 6–8).

the optical fibers discussed here, the cooling rate was 1 K/min and the samples were mounted on the stage with Ag paste (DuPont 4924 N).

E. Fiber strength measurements

It is well known that any crystallization in glasses can dramatically decrease the strength since it leads to sharp features that are effective stress concentrators. Fused silica optical fiber must be strong in order to survive the stresses it experiences during component fabrication and during service. Typical fiber is very strong ($\sim$5 GPa) but occasional weak defects are removed by proof testing at typically 350 or 700 MPa. Any crystallization in the fiber could degrade the strength below the proof stress and so would make the fiber unusable in conventional component designs. The mechanical properties of the fibers described here have therefore been characterized using industry standard test methods using both two-point flexure[11] and uniaxial tension.[12] Fused silica exhibits fatigue or stress corrosion cracking due to environmental moisture. For this reason all measurements have been made in a controlled environment at 23.0 ± 0.2 °C and $50\% \pm 3\%$ humidity.

III. RESULTS AND DISCUSSION

Figure 1 provides an optical micrograph of the conven-
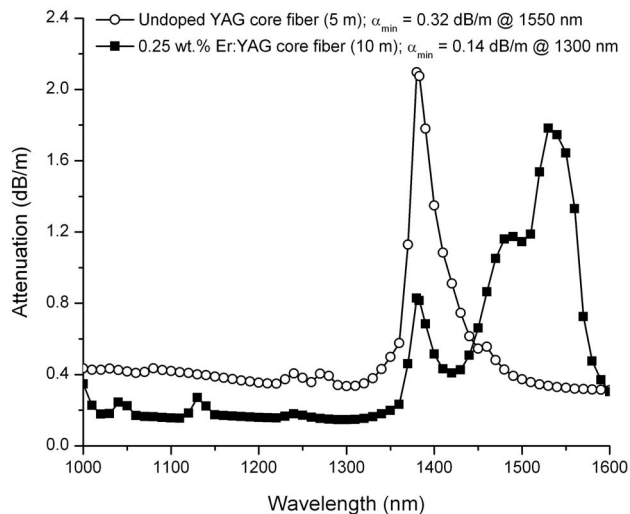
FIG. 2. Spectral attenuation of the undoped and lightly doped (0.25 wt % Er:YAG in the preform) "YAG-core" fiber. Absorption band peaked at 1385 nm is due to OH groups in the as-grown crystal.

tional (125 μm) fiber after fabrication. As can be seen, the core is central, circular, and guides light. The concentric cladding tubes that had been layered to provide the desired core/clad ratio were well fused.

Earlier iterations led to noncircular cores which most likely were due to ovalities in the starting cladding tubes. Since the core is molten at the draw temperatures, it would tend to flow and take on the shape of its "container." Light from a He–Ne laser (632.8 nm) propagated through a several meter length of 125 μm diameter fiber exhibited a far-field pattern consistent with a low-moded fiber ($4 < V < 6$) with a numerical aperture (NA) of approximately 0.38 and Δn $\sim$0.049. Given that the index of the core precursor YAG crystal exceeds 1.8 the measured NA clearly indicates a considerable amount of diffusion from the silica cladding into the (molten) core during draw. This is quantified in greater detail later in this paper.

In order to make an estimation of the spectral attenuation, a cutback measurement was made using a Photon Kinetics 2500 unit on selected lengths of 125 μm undoped and 0.25 wt % doped fibers. The results are shown in Fig. 2. A 5 m length of the undoped fiber exhibited a minimum loss (background attenuation) of about 0.33 dB/m at a wavelength of 1300 nm (where there is no OH or Er^{3+} absorption lines). A 10 m length of the lightly doped fiber exhibited a lower loss: about 0.14 dB/m at a wavelength of 1300 nm. These loss values are roughly 100 times lower than those achieved in Ref. 8 for a Cr-doped analog. The absorption due to the erbium dopant also is observed and is discussed in more detail below. In both cases, the peak at approximately 1385 nm is due to residual OH in the as-grown crystal from which the core rod was cut.

A higher resolution absorption spectrum for the fiber made from the 0.25 wt % Er:YAG is shown in Fig. 3. The figure is indicative of about 4.5 dB/m Er^{3+} peak core absorption (above the $\sim$0.15–0.2 dB/m background transmission loss) at 1532.5 nm for this low concentration fiber. The observed difference between the relatively low peak absorption
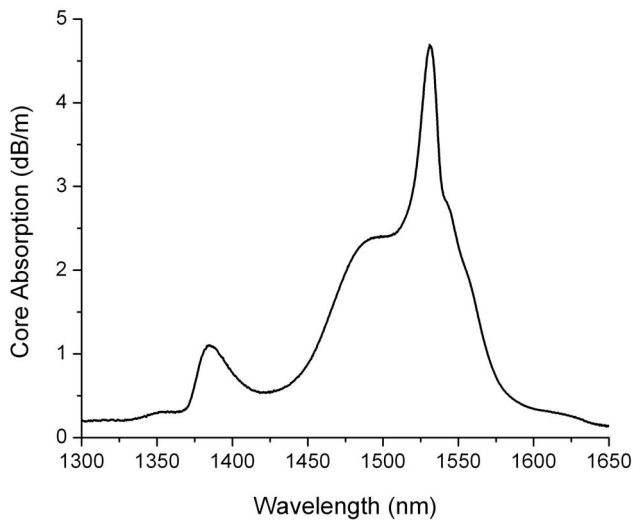
FIG. 3. Core absorption spectrum of the fiber drawn from the preform containing a 0.25 wt % Er:YAG crystal; 1 nm spectral resolution. Absorption peak at 1385 nm is also attributed to residual water absorption from the as-grown crystal.

values (~1.6 dB/m) in the Photon Kinetics 2500 attenuation measurement (Fig. 2) and true absorption measurements (Fig. 3) can be attributed to the highly under-resolved nature of the former. This difference is, as expected, the most prominent for the sharpest and narrowest 1532.5 nm absorption peak. Better resolution of the cutback measurement allows observation of the true spectral width of the major Er absorption peak in the fiber as well as any spectroscopic fine structure on the long-wavelength side of the absorption curve.

This is a quite reasonable level of transparency for such a nonoptimized initial study. In order to further characterize the optical properties of these fibers, the luminescence spectrum and luminescence lifetime were evaluated.

Figure 4 provides the absorption spectra of the YAG-derived fiber compared to that of single crystalline Er:YAG as well as two erbium-doped fiber amplifier (EDFA) fibers.
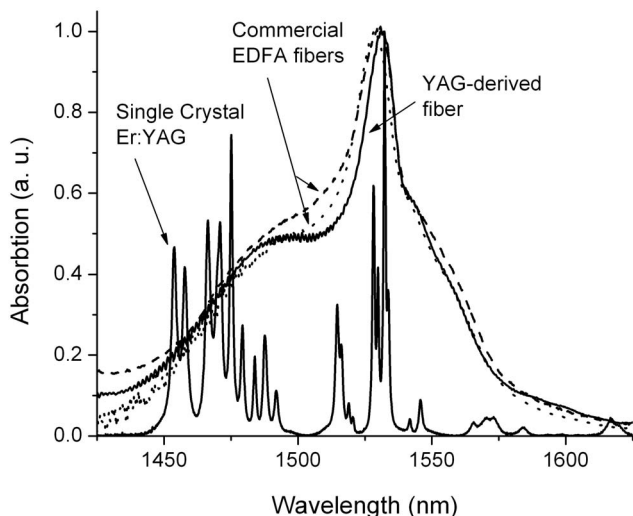
FIG. 4. Normalized absorption spectrum of the optical fiber derived from the Er:YAG containing preform compared to that for a YAG single crystal and two commercial EDFA fibers.
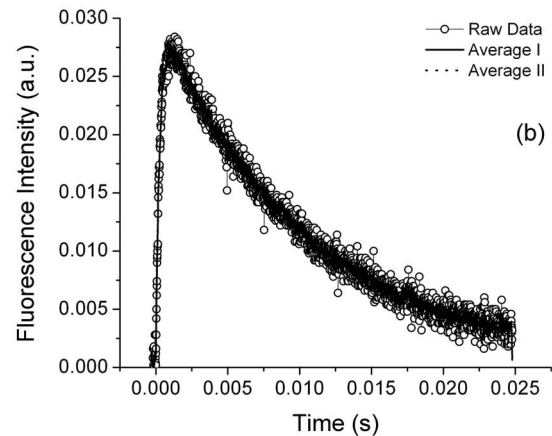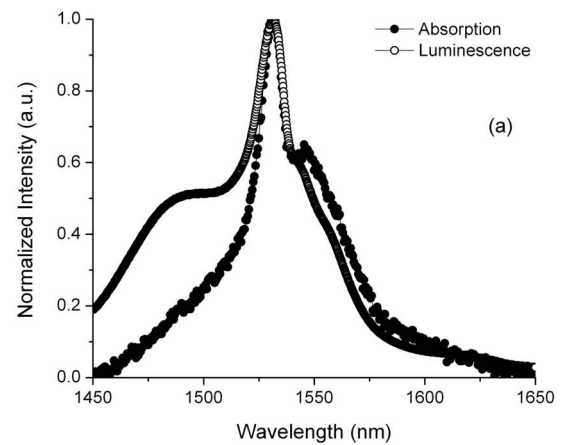
FIG. 5. Spectroscopic properties of the fiber drawn using the 0.25 wt % Er:YAG crystal in the core: (a) fluorescence corrected for spectral response of the spectrometer overlaid with the absorption of the fiber; (b) fluorescence kinetics of the 0.25 wt % Er^{3+}-doped fiber measured at 1532.5 nm with the ~10 ns pulse excitation at 532 nm.

The broad and "smooth" Er^{3+} absorption features in the drawn fiber versus those of the original Er:YAG in the preform implies a noncrystalline environment in the core of the drawn fiber. However, the observed linewidth is somewhat narrower than that of Er^{3+} doped into typical telecom-type aluminosilicate and germanosilicate glass hosts. These features can be seen in Fig. 4, which provides the normalized absorption spectra from the fiber derived from the Er:YAG containing preform compared to those from an Er:YAG single crystal and two commercial EDFA fibers.

Figure 5 provides the normalized $^4I_{13/2} \rightarrow {}^4I_{15/2}$ Er^{3+} fluorescence and absorption spectra [Fig. 5(a)] and the measured fluorescence intensity as a function of time [Fig. 5(b)]. Like Fig. 4, the spectra in Fig. 5(a) are indicative of an amorphous structure though the linewidth of the central peak is narrower than found in conventional EDFA glasses. Additionally, the ~10 ms first e-folding lifetime from the fiber is somewhat longer than the typical lifetime for Er-doped silica-based glasses. In order to better understand if there were any crystallographic considerations at play, x-ray diffraction and elemental analysis was performed.

Thicker fibers, due to the larger amount of core material relative to a thinner fiber, were analyzed using powder x-ray diffraction. In all cases, the cores were found to be x-ray

amorphous. This is in contrast to a previous report in the literature for a fiber fabricated using a fiber draw process,[9] which cites results on laser-heated pedestal grown fibers,[13] even though the formation processes and thermal histories are entirely different. The authors note the formation of crystalline γ-Al_2O_3 having an anomalously large unit cell parameter derived from selected area electron diffraction (0.856 nm versus the accepted value of 0.790 nm), which they attribute to the Cr doping. Such a large lattice expansion seems unlikely based on the low dopant concentrations reported (0.5 mol %) and the crystallite analyzed is more likely extremely Cr heavy or an alternative phase. The work does not provide sufficient detail to understand the chemical identity of the observed crystals or how they might result from the composition or fiber fabrication process.

In the present study, a manifestation of the amorphous nature of the core is found in the overlay of the absorption spectra of Er-doped YAG single crystal and Er-doped YAG-derived fibers (Fig. 3). Single-crystalline Er:YAG has very sharp, well defined, and mostly fully resolved, even at room temperature, absorption peaks which belong to different inter-Stark transitions between the $^4I_{15/2}$ and $^4I_{13/2}$ manifolds of Er^{3+} ions in YAG. Meanwhile, Er-doped YAG core fiber exhibits a smooth absorption contour with much less structure, and inter-Stark transitions mostly manifest themselves by little "shoulders" in the wings of the major absorption peak at 1532.5 nm, which is similar to Er-doped glass absorptions.

In order to further understand this, elemental mapping using the electron microscope was performed. The series of squares noted in Fig. 1(b) marks the locations where elemental analysis using EDX spectroscopy was performed. EDX provides the relative amounts of each element present in the region evaluated. Figures 6–8 provide the Si, O, Y, Al, and Er elemental profiles across the core and part of the glass cladding from the YAG ($Y_3Al_5O_{12}$)-derived fibers at each erbium doping level and a variety of fiber diameters. The specific fiber diameters at which the elemental analysis was performed were chosen arbitrarily.

There are a few interesting points to be made from Figs. 6–8. First, the presence of silicon (in the form of silica) in the core implies diffusion from the cladding into the core. This is reasonable to expect since one has a melt (the YAG core) in contact with a soft glass (the silica cladding) at elevated temperatures ($\sim$2050 °C). Diffusion is a thermally activated process and so the high processing temperatures for silica fibers further facilitate interdiffusion. Second, the smaller the core, the more silicon (i.e., silica) diffuses in from the cladding. This also is expected: the smaller the fiber, the shorter the diffusion length, the greater the concentration of the solute (diffusing species from cladding) in the solvent (core). Last, the compositional profiles are more steplike than expected for a diffusion-related process. This is likely due to the fiber fabrication process which promotes homogenization of the molten core as it transitions from the bulk preform through the neck down region and into the fiber where the composition is quenched into constancy.

An additional effect of silica diffusion from the cladding is that the core composition is "diluted." For example, the
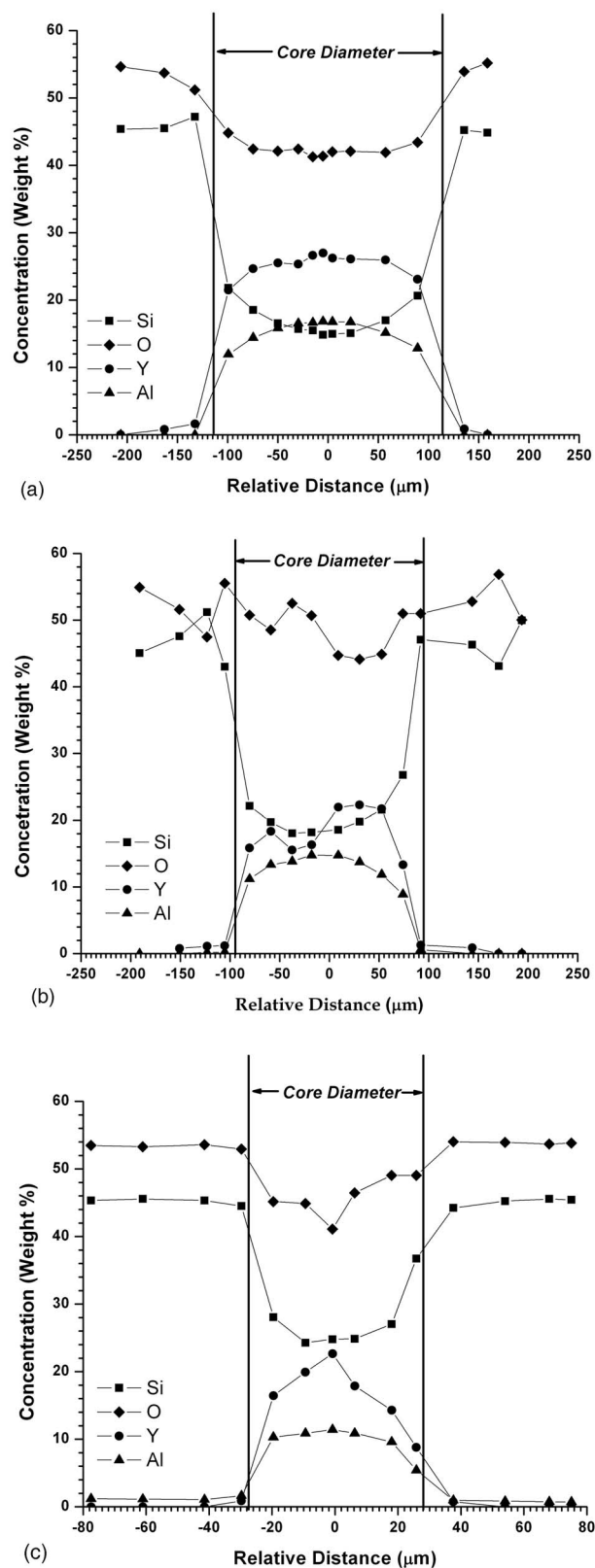
FIG. 6. Elemental profiles (relative elemental composition as a function of position across the fiber) for the undoped fiber. The figures (a), (b), and (c) were drawn to core sizes of 230, 191, and 57 μm, respectively.

fiber drawn from a preform containing 50 wt % Er:YAG exhibited about 20–25 wt % Er^{3+} in the final fiber, depending on the core size. While this dilution obviously reduces the amount of dopant in the fiber relative to that in the preform,
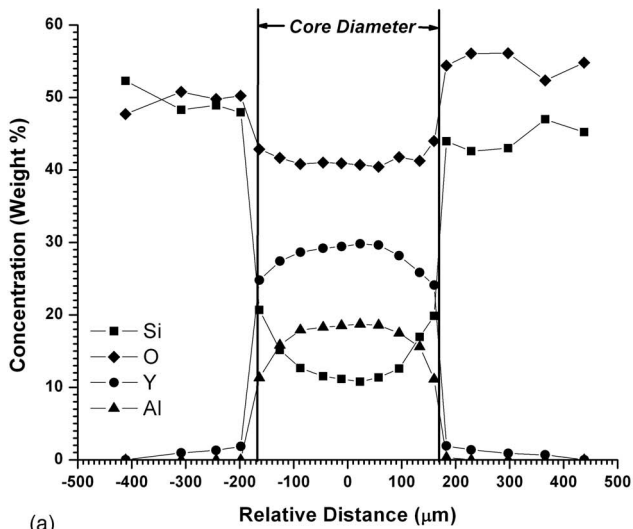
(a)
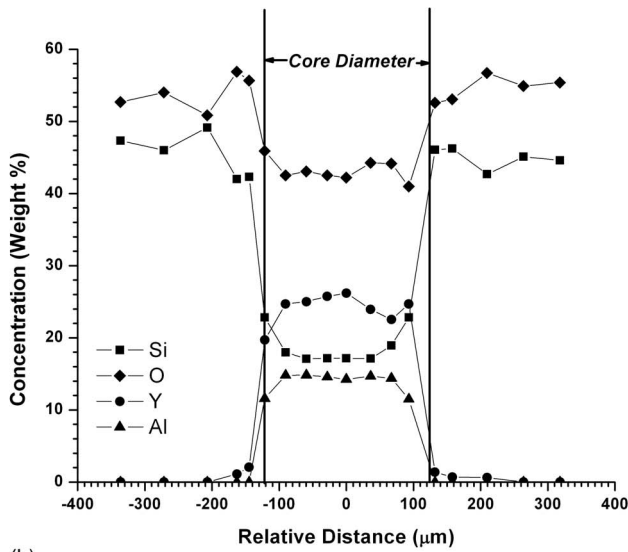
(b)
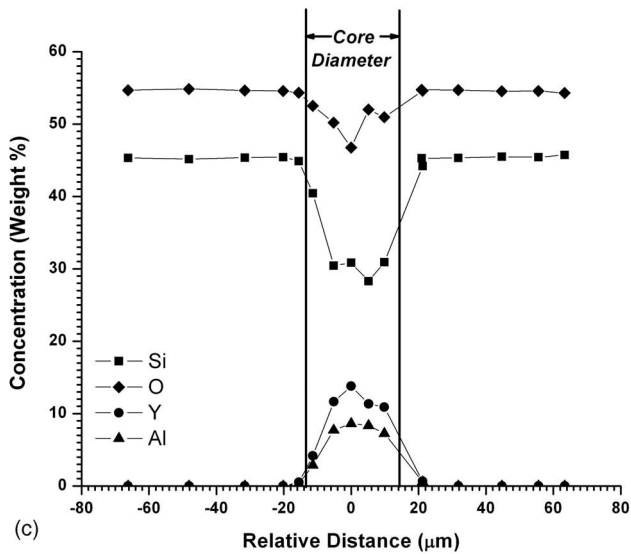
(c)

FIG. 7. Elemental profiles (relative elemental composition as a function of position across the fiber) for the for drawn from a preform containing 0.25 wt % Er:YAG. The figures (a), (b), and (c) were drawn to core sizes of 369, 248, and 24 μm, respectively. Note that the erbium concentration is too small to be measurement in this particular experiment.
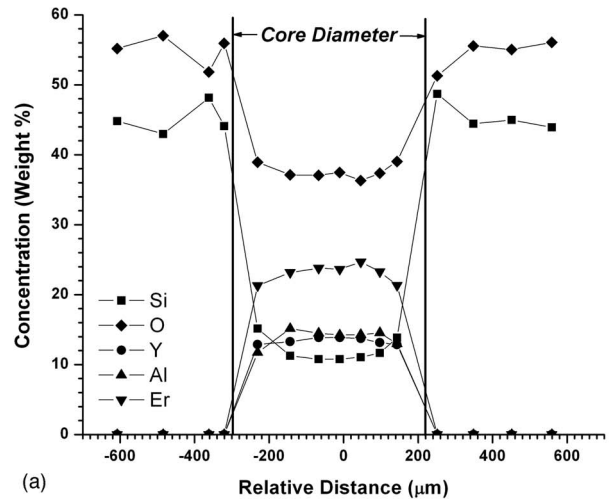
(a)
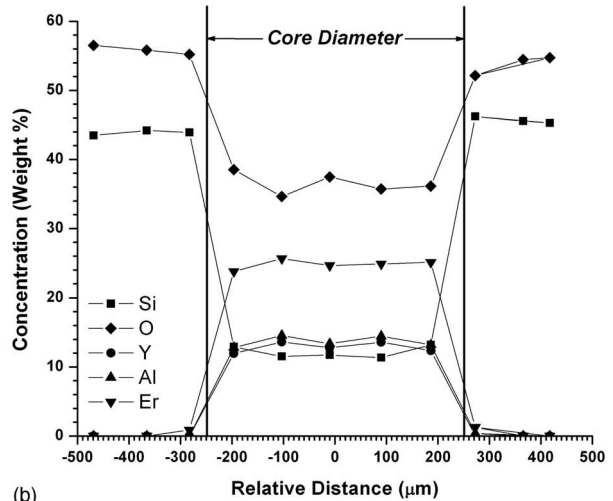
(b)
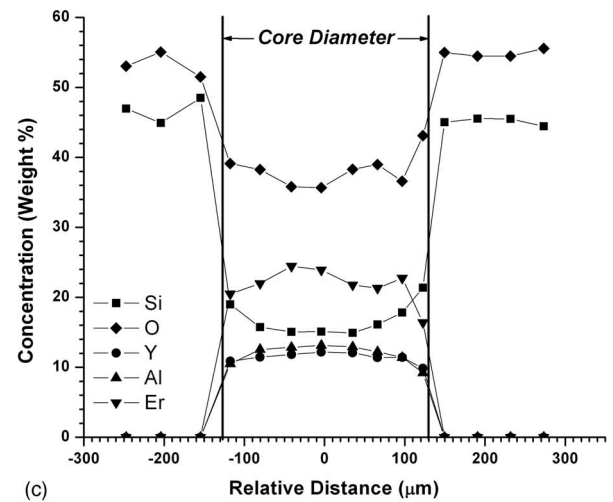
(c)

FIG. 8. Elemental profiles (relative elemental composition as a function of position across the fiber) for drawn from a preform containing 50 wt % Er:YAG. The figures (a), (b), and (c) were drawn to core sizes of 600, 500, and 260 μm, respectively.

nonetheless there is a considerably higher doping level than could be achieved under the more conventional methods employed to add rare earths into a fiber, e.g., solution doping and vapor-phase doping. Accordingly, this molten core ap-
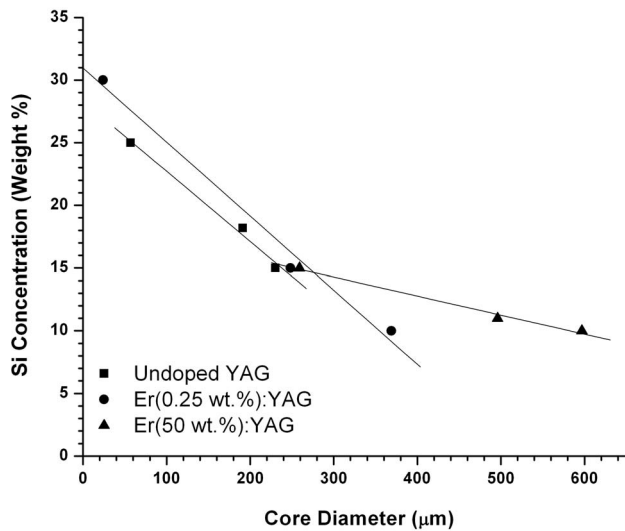
FIG. 9. Silicon concentration (indicating SiO_2 content) in the center of the fiber core taken from the data of Figs. 6–8. The lines are guides for the eyes.

FIG. 10. Thermal conductivity as a function of temperature measured along the fiber length.

proach could be used to yield doped fibers with unusually high rare-earth doping levels, even higher potentially than was achieved in Ref. 2.

Figure 9 is a compilation of the data from Figs. 6–8 and shows the concentration of silicon (as silica) at the center of each core of diameter noted. The lines are provided as a guide for the eyes and to show trends for the doped and undoped samples. Needless to say, the diffusivity of silica in each composition of molten YAG is slightly different and likely accounts for the measurable differences in concentration. If one was to take an average concentration at each diameter, then the silicon concentration decreases monotonically with increasing core size, hence diffusion length, as would be expected. A more in-depth evaluation of the interdiffusion between the molten YAG core and the glass cladding is underway and will be reported separately. The purpose here is to provide an initial quantification of the diffusion effects on core composition such that postulations could be made on the crystallography, or lack thereof, in these resultant fibers.

Even in the case of the largest core fiber, where the diffusion distance is longest, the center of the core possesses approximately 10 wt % silicon (as silica) from the cladding. The amorphous nature of the core then is likely due to some combination of two effects: (1) the presence of the silica in the YAG leads to a more stable yttrium aluminosilicate glass and (2) the significant quench rate ($\sim$2000 °C/s) of the melt to the solid during the fiber fabrication process prevents crystallization of the core. It is more likely that the composition (effect 1) plays the dominant role since equally high quench rates have recently been shown to still permit highly crystalline fibers utilizing similar draw techniques.[7]

Based on this recent success in fabricating crystalline core fibers via fiber draw techniques,[7] an original hope for this study was that silica-clad crystalline YAG core fibers could be realized. This would be of value to higher power amplifiers and lasers where thermal management and heat dissipation are critical. Even though the fibers were found to
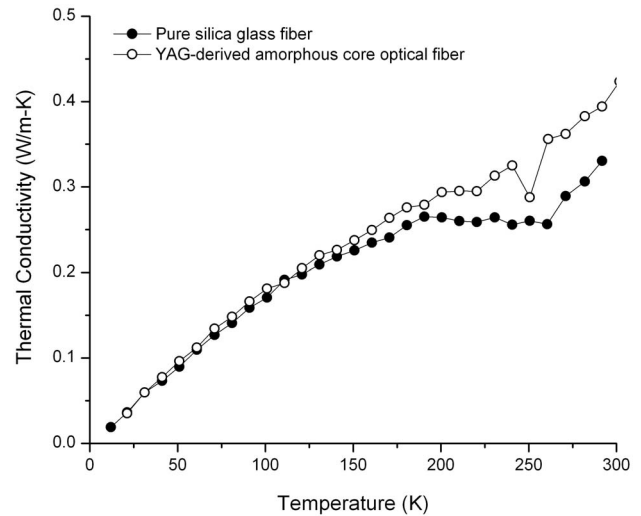
be amorphous, the thermal conductivity (Fig. 10) was measured as a function of temperature along a 4 cm length of the large core fiber. A bare glass silica fiber of equivalent diameter was drawn for direct comparison.

At low temperatures, the fiber derived from the YAG core preform exhibits equal thermal conductivity to that of a conventional silica-based optical fiber. This is not particularly surprising because of the small core-to-clad ratio; hence the fiber is principally silica. However, at temperature approaching room temperature, there is a deviation and the fiber derived from YAG exhibits a thermal conductivity along its length that is $\sim$20% higher than a conventional silica fiber. The reason for this enhanced thermal conductivity is unclear to date but is reproducible and is a subject for continued study.

In order to fully characterize these fibers, their mechanical properties also were investigated. Figure 11 shows the results of two-point bend strength measurements on the undoped YAG fiber. The results are graphed on a Weibull probability plot $\ln\ln[1/(1-P_f)]$ versus $\ln\sigma_f$, where P_f is the
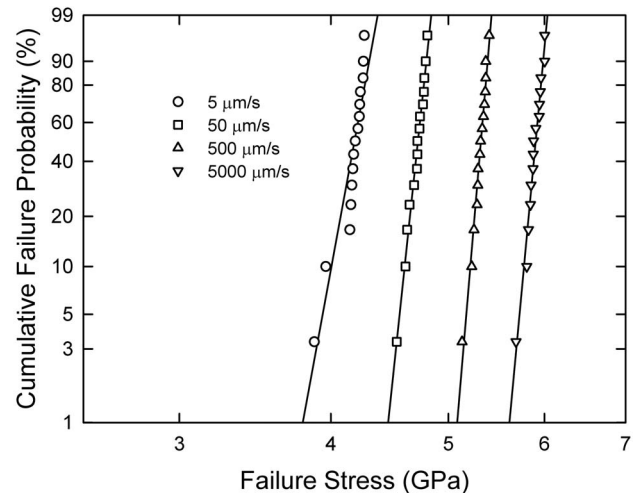
FIG. 11. Weibull probability plot of the strength of undoped fiber measured in two-point bending at four different faceplate speeds.
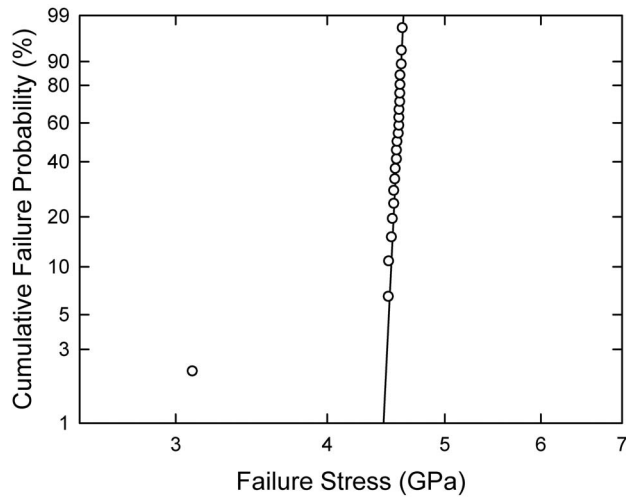
FIG. 12. Weibull probability plot of the strength of fiber drawn from the 50% Er:YAG containing preform measured in uniaxial tension at a stress rate of 30 MPa/s.

cumulative probability of failure and σ_f is the failure stress. This plot is widely used to visualize strength distributions. In this case all four distributions are narrow as is typical of fused silica optical fiber. The strength is measured at four faceplate speeds in order to characterize the stress corrosion cracking behavior which occurs in the humid environment. The stress corrosion susceptibility parameter, n, calculated from these data is 20.9 with a 95% confidence interval of 20.2–21.6. Again, this behavior is very typical of fused silica optical fiber.

However, two-point bending is not sensitive to the presence of large defects in the core of the fiber, such as might be produced by crystallization or residual bubbles from the core melt, since the stress at any point in the bent fiber is proportional to the distance from the neutral axis, i.e., the distance from the center of the core. For a ~ 6 μm diameter core and a 125 μm diameter fiber, the stress at the core/clad interface is only $\sim 0.05\%$ of the maximum stress at the surface of the fiber. For this reason the strength has been characterized using uniaxial tension using a 0.5 m gauge length in which the entire volume of the fiber is subjected to the same stress. Figure 12 shows the results for the strength of fiber derived from the 50% Er:YAG measured at a stress rate of 30 MPa/s. Except for one weaker specimen at ~ 3 GPa, the strength distribution is narrow with values typical of fused silica. The broken ends of the weaker specimen were recovered and examined in the optical microscope. The two fracture surfaces were not mirror images of each other meaning the fiber shattered locally at failure, as is typical for strengths above ~ 1 GPa. Fractographic analysis was therefore unable to determine the position of the flaw causing failure. This weaker specimen could have been caused by a defect at the surface of the glass, which can occasionally occur, or at the core/clad interface. In either case the impact on reliability is not great—the strength of 3 GPa is much higher than typical proof stresses (typically 0.36–0.72 GPa) so the strength limiting defect would not cause failure during either proof testing or subsequent service. Further, if the flaw is indeed caused by the presence of a defect in the core, it is less

severe than a flaw of an equivalent size at the surface because it is not exposed to environmental moisture and so will not fatigue due to stress corrosion.

While no severe defects were detected in the ~ 15 m of fiber tested here, there is a possibility of very large flaws if much longer lengths of fiber were examined. Unlike the other properties of the fiber described here, which are average properties along the length of the fiber, strength depends on the extreme values of flaw sizes in the test length and so is well known to be length dependent. However, these early results on this fiber do conclusively show that the rapid quenching of a molten core during draw does not necessarily degrade the strength to the point where the fiber is unusable, at least on the length scale of tens of meters.

Residual issues and considerations

The purpose of this paper was to provide a more in-depth analysis of the materials and physical properties of glass-clad optical fibers derived from a crystalline (YAG) core containing preform. As with any initial study, there are a number of future efforts worth pursuing. More specifically, the following studies and developments would enable such fibers to be of greater value to the community:

(i)   Determine through time, temperature, and transformation thermal studies if it is possible to develop YAG crystallinity (or polycrystallinity) of the core. If polycrystallinity is achievable, then develop approaches to minimizing the grain size in order to optimize fiber transparency. Here previous work on glass ceramic optical fibers might be useful.[14]

(ii) There is a need for better understanding of the advantages and disadvantages of diffusion and other ways to control it (e.g., draw temperature, draw time, intermediate cladding layers as diffusion barriers, etc.). Given the inevitability of diffusion, how might it be minimized or, at least, insightfully used to end with a core composition that provides desirable optical properties? The work in Ref. 7 proves that high degrees of crystallinity can be obtained in molten core-derived optical fibers even given moderate degrees of diffusion.

(iii) Determine the application-specific balance between larger core size (i.e., less diffusion) and fiber flexibility.

(iv) Develop approaches for tailoring the fiber NA for single mode operation as well as achieving more complex fiber designs.

(v)   Continue to investigate the broadened range of materials and compositions permitted by such nonequilibrium molten core approaches to optical fibers.

IV. CONCLUSIONS

An in-depth analysis of optical fibers derived from a preform containing crystalline YAG as the starting core material. Conventional fiber draw parameters led to a core that was amorphous, which likely results from in diffusion of silica from the cladding. Regardless, the resultant fibers ex-

hibited background loss figures of ~0.1–0.3 dB/m, room temperature thermal conductivity along its length that was roughly 20% higher than conventional optical fiber, and mechanical properties equivalent to standard optical fiber. The spectroscopic properties of Er^{3+} doped into the precursor YAG corroborated the amorphous nature of the core material though the linewidth is somewhat narrower and fluorescence lifetime is somewhat longer than that in conventional silicate glasses. Efforts should continue to further evaluate the influence of processing conditions on core crystal composition (i.e., diffusion) and the potential development of a crystalline or polycrystalline core.

[1] E. Snitzer and R. Tumminelli, Opt. Lett. **14**, 757 (1989).
[2] J. Ballato and E. Snitzer, Appl. Opt. **34**, 6848 (1995).
[3] N. Goel, R. Stolen, S. Morgan, J.-K. Kim, D. Kominsky, and G. Pickrell, Opt. Lett. **31**, 438 (2006).
[4] M. Fejer, J. Nightingale, G. Magel, and R. Byer, Rev. Sci. Instrum. **55**, 1791 (1984).
[5] G. A. Magel, D. H. Jundt, M. M. Fejer, and R. L. Byer, Proc. SPIE **61B**, 89 (1986).
[6] C. Lo, K. Huang, J. Chen, S. Tu, and S. Huang, Opt. Lett. **29**, 439 (2004).
[7] J. Ballato, T. Hawkins, P. Foy, R. Stolen, B. Kokuoz, M. Ellison, C. McMillen, J. Reppert, A. M. Rao, M. Daw, S. Sharma, R. Shori, O. Stafsudd, R. R. Rice, and D. R. Powers, Opt. Express **16**, 18675 (2008).
[8] Y. Huang, Y. Lu, J. Chen, Y. Hsu, Y. Huang, S. Huang, and W. Cheng, Opt. Express **14**, 8492 (2006).
[9] Y.-C. Huang, J.-S. Wang, Y.-K. Lu, W.-K. Liu, K.-Y. Huang, S.-L. Huang, and W.-H. Cheng, Opt. Express **15**, 14382 (2007).
[10] B. M. Zawilski, R. T. Littleton, and T. M. Tritt, Rev. Sci. Instrum. **72**, 1770 (2001).
[11] TIA/EIA TSB 62–13, Telecommunications Industry Association, ITM, Washington, DC, 2000.
[12] TIA/EIA-455–28-C, Telecommunications Industry Association, FOTP, Washington, DC, 1999.
[13] C.-Y. Lo, K.-Y. Huang, J.-C. Chen, C.-Y. Chuang, C.-C. Lai, S.-L. Huang, Y.-S. Lin, and P. S. Yeh, Opt. Lett. **30**, 129 (2005).
[14] B. N. Samson, P. A. Tick, and N. F. Borrelli, Opt. Lett. **26**, 145 (2001).